In-line laser Doppler velocimeter using fibre-optic Bragg grating interferometric filters

In-line laser Doppler velocimeter using fibre-optic Bragg grating interferometric filters

E Chehura, C-C Ye and R P Tatam[1]

Optical Sensors Group, Centre for Photonics and Optical Engineering, School of Engineering,
Cranfield University, Cranfield, Bedford MK43 0AL, UK

E-mail: r.p.tatam@cranfield.ac.uk

Abstract

An all fibre-based laser Doppler velocimetry system for the measurement of the predominantly on-axis component of velocity is presented. The technique employs Bragg grating-based Fabry–Perot interferometric filters custom-designed to suit the transduction of Doppler optical frequency shifts to intensity. The sensitivity of the in-fibre filters to strain is exploited to provide tuning of the filter relative to the centre wavelength of the laser and of the spectral shape of the filter, which in turn varies the velocity range, sensitivity and resolution. A phase-locking scheme incorporated to stabilize the filter is described together with a laser-wavelength stabilization system that locks to a Doppler-broadened absorption line of iodine vapour. An optical fibre-linked probe head is used to couple the laser beam at 514.5 nm to and from the measurement volume. The velocimeter is characterized by measuring the velocity of a rotating disc over ranges of ±42 and ±7 m s^{-1} with a resolution of 0.2 m s^{-1}.
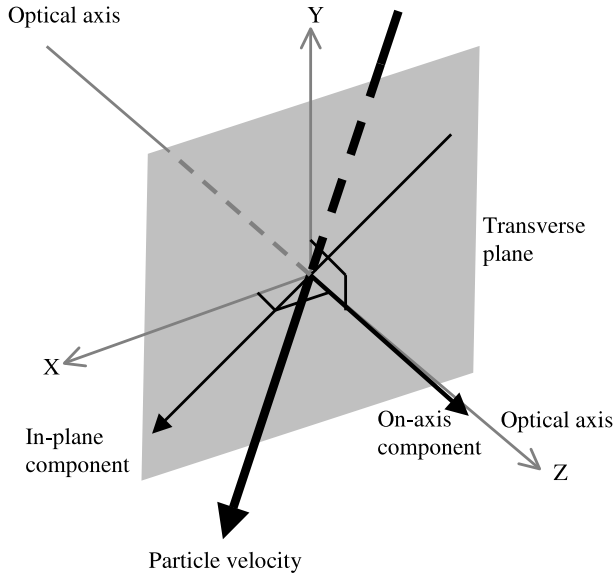
1. Introduction

There is increasing demand to accurately measure all three components of fluid velocity as complete three-dimensional characterization of complex fluid flow phenomena is only available from advanced computational fluid dynamic models (CFD codes) whose validation relies on the availability of experimental data. Optical instrumentation is the main focus of research activities, motivated by its non-intrusive nature to the flow and its applicability in harsh environments.

Optical techniques measure velocity either at a localized point or across a plane defined by a laser light sheet. Laser Doppler velocimetry (LDV), or laser Doppler anemometry (LDA), was the first optical technique to measure fluid velocity at a localized point. The principle is based on measuring the Doppler shift in an optical frequency imposed on the

illuminating laser light by moving particles entrained in the flow [1]. LDV measures the Doppler shift by heterodyning two light beams with one scattered from the particles and the other acting as a reference (reference beam technique) [2] or both beams scattered from the flow (Doppler difference technique) [3]. Reference beam LDV is most suited to the measurement of the on-axis component of velocity (figure 1) whilst transverse velocity components (figure 1) are more readily measured by Doppler difference LDV [4] and laser two-focus anemometry (L2F) [5]. The L2F principle is based on the measurement of the time of flight of a particle crossing a light gate formed in the flow by two highly focused laser beams. To obtain the three components of velocity with equal resolution for each component requires a system that directly measures the three orthogonal components. Such a system requires at least two orthogonal entrance ports to the measurement volume. In many practical applications this is difficult to achieve experimentally and is not achievable

---

[1] Author to whom any correspondence should be addressed.

Figure 1. Illustration of three orthogonal components of velocity.

Figure 2. Measurement principle of the Doppler frequency shift using an iodine absorption line.

Figure 3. Measurement geometry of the Doppler frequency shift.

where optical access is limited, for example in turbomachinery applications where access is usually restricted to a single window [6]. A commercial system uses three Doppler difference channels and a single probe head [7], thus measuring non-orthogonal components of velocity [8]. The disadvantage of the configuration is that the small angle between the measured components introduces a large uncertainty in the on-axis component. These difficulties have led to a number of methods to measure three velocity components using a single probe head. A fibre-optic probe using two Doppler difference channels, to measure the x and y components, and a reference beam channel to measure the z component has been reported [4, 9]. The use of fibre optics overcomes the problems of alignment encountered in a bulk optic reference beam system, but the velocity range is limited due to the high frequency of the measured signal even for moderate velocities, e.g. a 100 MHz processor is required for approximately 30 m s^{-1} at a wavelength of 514.5 nm. The measurement of higher velocities has been investigated using the filter characteristics of atomic and molecular gases [10]. The principle of filter-based LDV is shown in figure 2. The laser source is tuned to the middle of one side of the absorption line such that the normalized scattered intensity is attenuated to half full transmission for zero velocity measurement. Any Doppler shift, $\Delta\nu$, will be measured as a change in the measured intensity while its sign determines the sign of the measured velocity. The velocity, V, for the flow is calculated from the Doppler shift using [11]

$$\Delta\nu = \frac{\nu_0}{c} \cdot (\hat{o} - \hat{i}) \cdot V \qquad (1)$$

where ν_0 is the initial optical frequency of the laser, c is the free space speed of light and $\hat{o}$ and $\hat{i}$ are unit vectors in the observation and illumination directions respectively (figure 3).

Although originally used for the planar technique of Doppler global velocimetry (DGV), sometimes known as planar Doppler velocimetry (PDV) [12], iodine vapour cell based filters have also been used to measure the in-line velocity
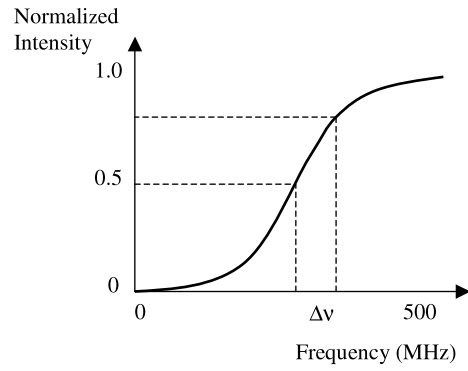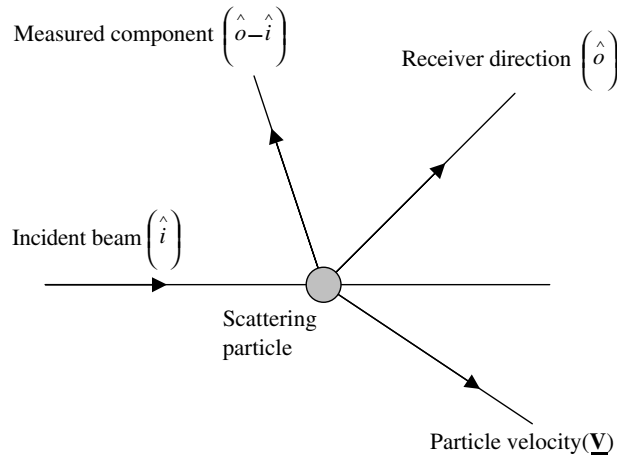
component [13–16]. Optical configurations to measure the on-axis velocity component using limited optical access remain the subject of research [2, 9, 13–18].

This paper investigates an in-line laser Doppler velocimeter based on the use of a Bragg grating Fabry–Perot (FP) interferometric filter to measure the Doppler frequency shift. The directional discrimination of the velocity is automatic, as is the case with the iodine cell but not with LDV where a Bragg cell is normally used. The filter response is tuneable via strain, thus adjusting the velocity range, resolution and sensitivity to match different flow regimes. The Bragg grating centre wavelengths can be chosen to match any required laser emission wavelength. Two independent stabilization systems were implemented to control the phase of the fibre-optic interferometer and the wavelength of the laser.

2. In-fibre Bragg grating technology

An in-fibre Bragg grating (FBG) is a refractive index grating that acts as a narrow band spectral filter, reflecting light at a particular (Bragg) wavelength [19]. The FBG is fabricated by the exposure of the core of a single-mode optical fibre to an interference pattern formed between two interfering UV beams that create a refractive index modulation (figure 4) in the fibre core. A reflected signal and a notch in the transmission spectrum, both with narrow bandwidths centred at the Bragg
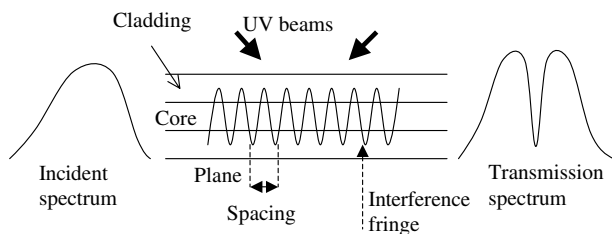
Figure 4. The formation and principle of operation of an FBG.

wavelength, are obtained when the grating is illuminated from a source with a broad optical bandwidth. The maximum reflectivity of the grating occurs when the phase-matching (Bragg) condition is satisfied, which is given by [20]

$$p\lambda_B = 2n_{eff}\Lambda \qquad (2)$$

where p is the order of interaction, λ_B is the Bragg wavelength, n_{eff} is the effective refractive index of the guided mode and Λ is the grating period. A typical spectral bandwidth of an unchirped grating of a few millimetres in length is about 0.2 nm, which corresponds to about 227 GHz in optical frequency at a wavelength of 514.5 nm. This renders the Bragg grating very insensitive as a frequency to intensity transducer as typical Doppler frequency shifts are of the order of a few hundred megahertz.

It is therefore necessary to consider interferometric filters whose frequency bandwidths can be fabricated in the range 0.1–1 GHz. We have investigated such filters by way of computer models based on the transfer matrix approach [21, 22]. In addition to a narrow bandwidth, the filter should have a linear and steep slope, high visibility, and good stability to environmental perturbations particularly temperature. The model has shown that the FP interferometer [23], distributed feedback grating (DFG) [24] and the moiré grating [25] are suitable for flow measurement applications. A moiré grating results from the superposition of two gratings with slightly different centre wavelengths while a DFG filter is produced by incorporating a phase step within a grating structure. Figures 5(a) and (b) show the result of a transfer matrix model for a DFG filter of 4 mm in length with a π phaseshift in the middle producing a passband transmission of 425 MHz (full width half maximum, FWHM) for a refractive index modulation of 2.5×10^{-4}. The model was also applied to two superimposed 4 mm long gratings with a centre wavelength difference of 0.0115 nm at 514.5 nm to produce a moiré grating that resulted in a passband of 400 MHz (FWHM) for a refractive index modulation of 7.5×10^{-5} (figures 6(a) and (b)). The transfer matrix model for an FP filter consisting of two 4 mm long gratings with 60% reflectivity, each with refractive index modulation of 4×10^{-5}, and separated by 50 mm, resulted in a passband transmission of 340 MHz (FWHM) and a free spectral range (FSR) of 1.92 GHz (figures 7(a) and (b)). The chosen grating length and reflectivity are representative of what is readily achievable in grating fabrication experiments. Filters with bandwidths as narrow as 100 MHz have been fabricated; e.g. a DFG filter was produced by UV post-processing of a 4 cm uniform period grating that had a refractive index modulation of 1.8×10^{-5} written using a point by point technique [26] thus confirming the experimental feasibility of the fabrication
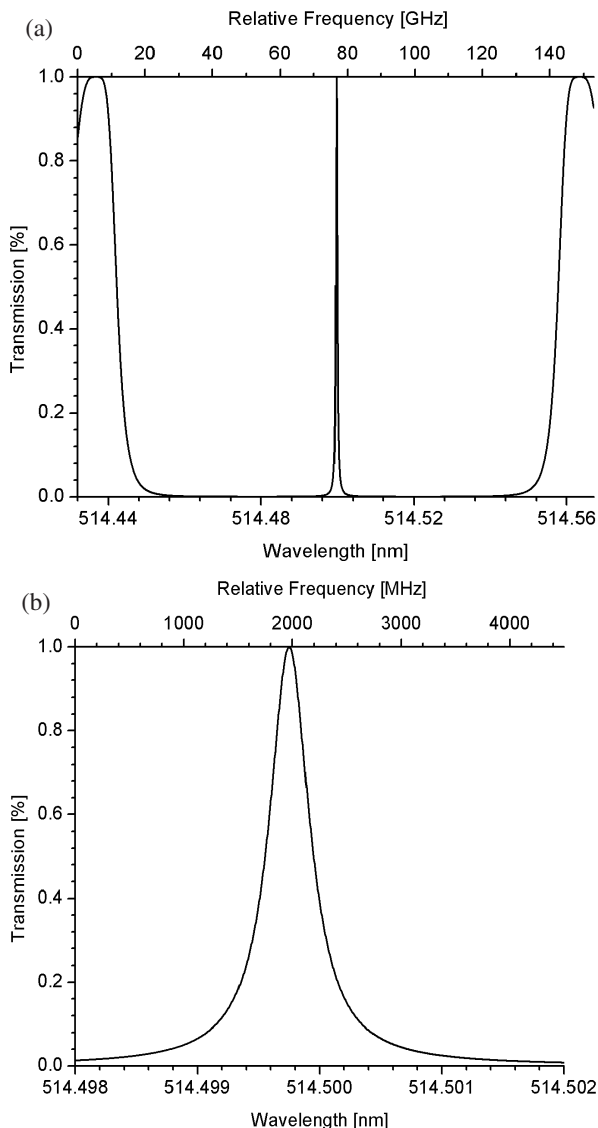
Figure 5. (a) Passband transmission of a π phaseshifted grating (DFG filter) that is 4 mm long having a refractive index modulation of 2.5×10^{-4}. (b) Passband transmission (extracted from figure 5(a)) with FWHM bandwidth of 425 MHz.

process. The DFG and moiré grating based interferometric filters can be very short (~5 mm), which is attractive for stabilization against environmental perturbations, particularly temperature. All these filters, particularly the DFG, can be accurately fabricated using phase masks but these are generally expensive to acquire and will have to be custom made for the 514.5 and 532 nm emission wavelengths of commonly used argon-ion and frequency-doubled Nd: YAG lasers. In contrast an FP filter may be readily fabricated without the use of a phase mask and it is this type of filter that is investigated experimentally here (figure 8).

Figure 9 is the result of a theoretical model that shows the variation of filter sensitivity as given by the gradient of the linear portion of a flank of the transfer function as a function of the FSR of an FP filter at constant finesse. The graph, at a finesse of 4.7 (described further in section 3), shows that the fibre-optic filter will always have higher sensitivity than an iodine cell if it is fabricated at an FSR of less than about
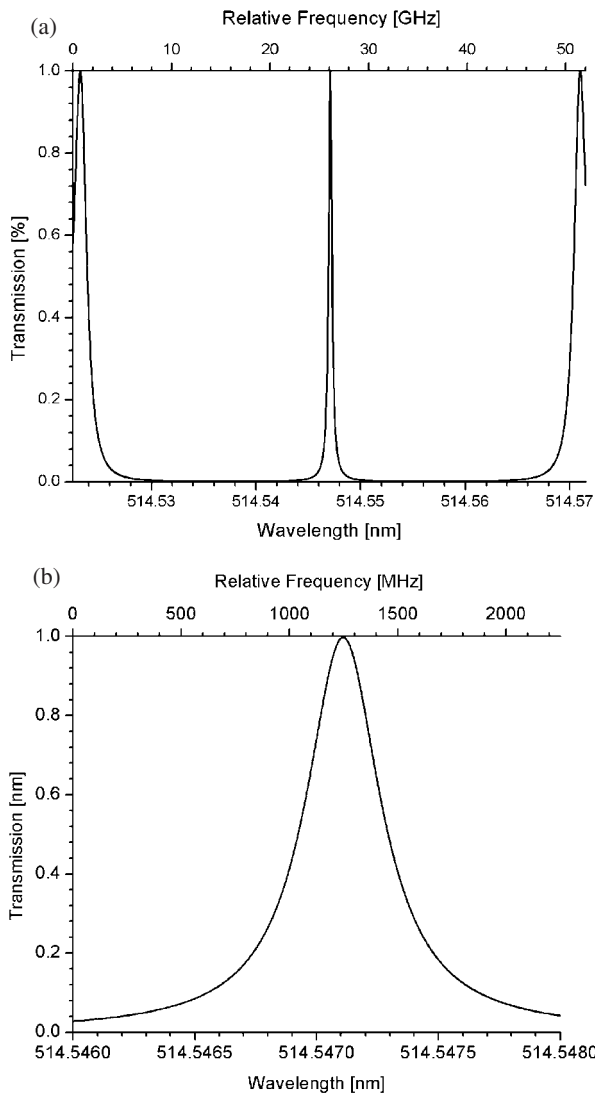
Figure 6. (a) Passband transmission from a moiré grating consisting of two superimposed 4 mm long gratings with centre wavelength difference of 0.0115 nm at 514.5 nm with refractive index modulation of 7.5×10^{-5}. (b) Passband transmission (extracted from figure 6(a)) with FWHM bandwidth of 400 MHz.

3 GHz. A filter of about 1.6 GHz in FSR will have about twice the sensitivity when compared with an iodine cell with a bandwidth of approximately 1.6 GHz and sensitivity of about 1.96 GHz^{-1}. Higher finesse will produce higher sensitivity.

3. Experimental details

3.1. In-fibre Bragg grating fabrication

The filter transfer function characteristics were required to have steep and linear slopes for high velocity sensitivity and linear frequency to intensity transduction respectively. High-finesse filters with small passband frequencies are preferable for high velocity resolution but at the expense of reduced velocity ranges. The bandwidth sets the maximum measurable Doppler frequency shift thus setting a limit to the measured velocity range (figure 10). The FSR defines the optical frequency difference between any two adjacent fringes and is inversely
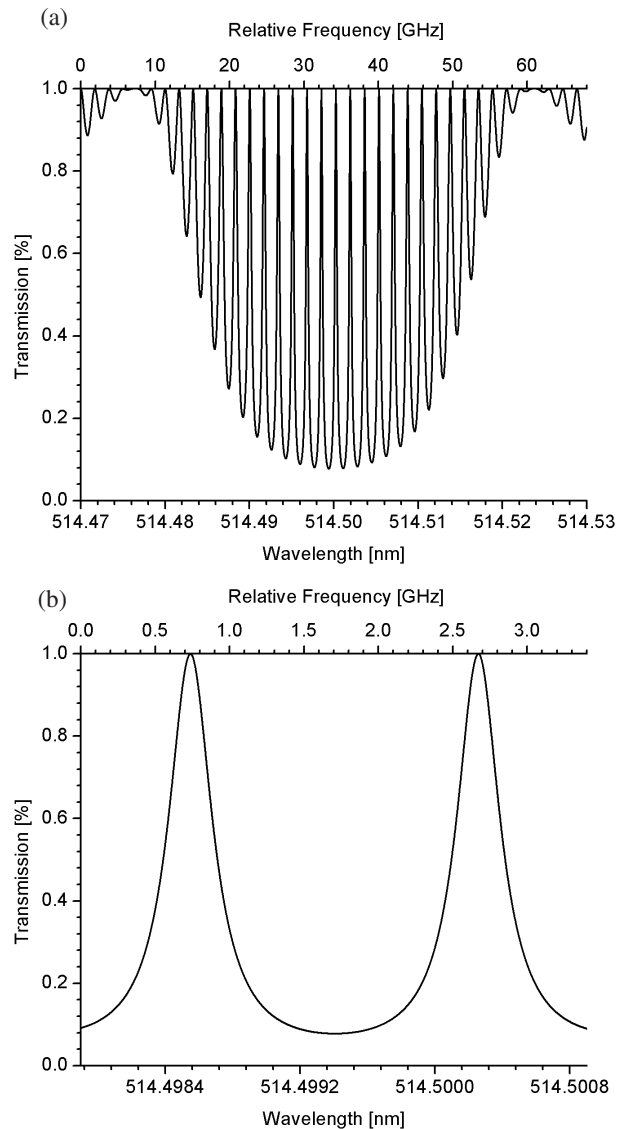

Figure 7. (a) Passband transmission of a FP filter consisting of two 4 mm long gratings with 60% reflectivity, each with refractive index modulation of 4×10^{-5}, and separated by 50 mm. (b) Passband transmission (extracted from figure 7(a)) with FWHM bandwidth of 340 MHz and a FSR of 1.92 GHz.
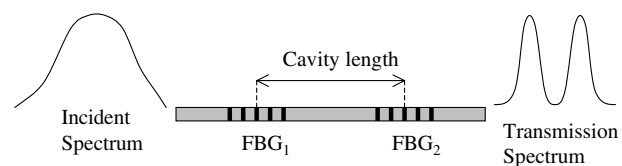
Figure 8. Illustration of an FBG FP cavity and its principle of operation.

dependent on the FP cavity length. Low-FSR filters are prone to environmental perturbations because of their large length and a compromise is to use a larger FSR and thus a relatively larger velocity range. The finesse of the filter, defined as the ratio of the FSR to the passband frequency bandwidth at FWHM transmission, describes the sharpness of the fringes and is controlled by the reflectivity of the grating.
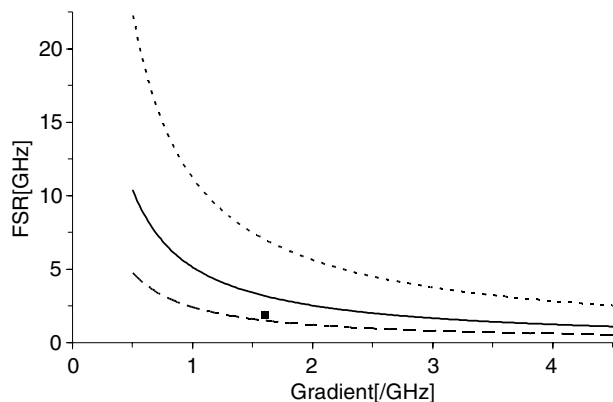
Figure 9. Filter sensitivity as a function of FSR at different finesse, f: ■, approximate FSR of iodine cell; ······, $f = 9.6$; ——, $f = 4.7$; — — —, $f = 2.9$; FSR, free spectral range.
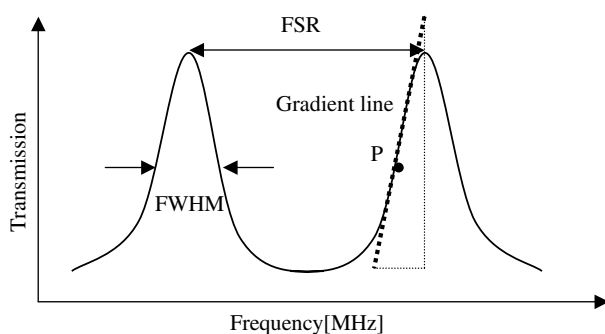
Figure 10. Typical transfer function of an FP filter describing its important parameters: P, point of maximum gradient; FWHM, full width at half maximum bandwidth, FSR, free spectral range.

Two Bragg gratings, of approximately 40% reflectivity and separated by 63 mm, were interferometrically fabricated in a single-mode fibre (Fibrecore SM450) at the argon-ion laser wavelength of 514.5 nm using an ultraviolet (UV) beam at 245 nm in a holographic side-writing technique [19, 27] thereby forming an FP filter with an FSR of 1.6 GHz, FWHM bandwidth of 480 MHz, and finesse of 3.3. Such a low finesse filter trades off the low velocity resolution for a relatively larger velocity range of about 200 m s^{-1}. The transfer function of the FP filter with a bandwidth of 1.6 GHz could only be measured by straining the filter. Both gratings are tuned to the laser wavelength by the application of strain via piezocontrolled translation stages after which one grating is modulated by a small-amplitude triangular or sawtooth voltage (figure 11(a)). The signal transmitted through the filter (figure 11(b)) drifted but could be periodically reset by the application of a small offset strain on one grating. This signal fading was a combination of laser wavelength drift and the effects of environmental perturbations on the filter. The centre wavelength of each grating was separately tuned via strain, thus changing the reflectivity producing a concomitant variation in the shape of the transfer function of the filter. Figure 12, for example, shows the experimental adjustment to passband bandwidth FWHM over the range, 0.27–0.62 GHz, sensitivity over the range, 0.5–1.40 GHz^{-1}, and visibility over a range of 15–22%. The transfer function of an FP interferometer is theoretically described by a Voigt function [28, 29], which is itself a convolution of Gaussian and Lorentzian functions. The

Voigt function approximates closely to a Lorentzian at high finesse and a Gaussian at low finesse [29]. The continuous (spectral) line in figure 12 is a fit of the Gaussian function onto the experimental data of the transfer function for a finesse of 3. The graph shows a good fit to the data with chi square and R^2 values of 5.0969×10^{-6} and 0.999 01 respectively where R is the correlation coefficient.

3.2. Laser wavelength stabilization

The source used was an argon-ion laser (Spectra Physics 2060-10), the output wavelength of which can be controlled by two independent frequency stabilization mechanisms for slow (Z-lock) and rapid (J-lock) frequency drifts respectively. The stabilized laser has a linewidth of about 3 MHz and an overall residual optical frequency jitter of approximately 2 MHz. The frequency–temperature coefficient of the laser is 50 MHz °C^{-1} and typical drifts of the order of 600 MHz were observed over time durations of about 2 h under normal laboratory conditions. The drift and jitter in the centre wavelength of the laser causes the operating point of the interferometer to change. In addition the fibre-optic FP filters fabricated had narrow FWHM frequency bandwidths with a tuning range of about 250–650 MHz, small enough to be highly sensitive to wavelength fluctuations. An additional active feedback stabilization system was therefore required to stabilize the laser wavelength to thermal fluctuations. An active feedback control-loop was designed to lock the laser wavelength to a 50% transmission point on a Doppler broadened absorption line of molecular iodine vapour enclosed in a glass cell [30]. Figure 13 shows a schematic diagram of the experimental layout in which a single-mode directional coupler with a split ratio of 50:50 was used. The iodine cell consisted of a main body that was maintained at 55 °C and a cold finger at 40 °C, a condition that resulted in 100% transmission depth and 1.76 GHz^{-1} slope of the absorption line. The iodine cell and proportional-integral-derivative (PID) temperature controller were built in-house for a related full-field planar Doppler velocimeter (PDV) [31].

The photodiode outputs were connected to a custom-designed electronic controller. The first stage of this controller consisted of an analogue divider circuit that normalized the two detector signals to remove laser intensity fluctuations as well as dark noise, with the remaining fluctuations accounting for the laser wavelength change. The next stage of the circuit generated an error voltage that was proportional to laser wavelength fluctuations or drift. Three other circuits acting as proportional, integral and derivative controllers (PID) were designed to act upon the generated error voltage, the result of which was fed back to the laser via the existing Z-lock electronics of the laser. The Z-lock electronics generated a voltage that either heated or cooled the intracavity FP etalon, thereby adjusting its cavity length.

The control range required was 1 GHz (±500 MHz) of optical frequency change corresponding to a voltage control of 0.24 V. The accuracy of control was required to be 0.24 mV to achieve a frequency stability of 1 MHz. A 0.002 change in iodine cell transmission was equivalent to a 1 MHz change in frequency. The aim was to achieve a velocity resolution of better than ±0.2 m s^{-1}, that required ±1 MHz frequency
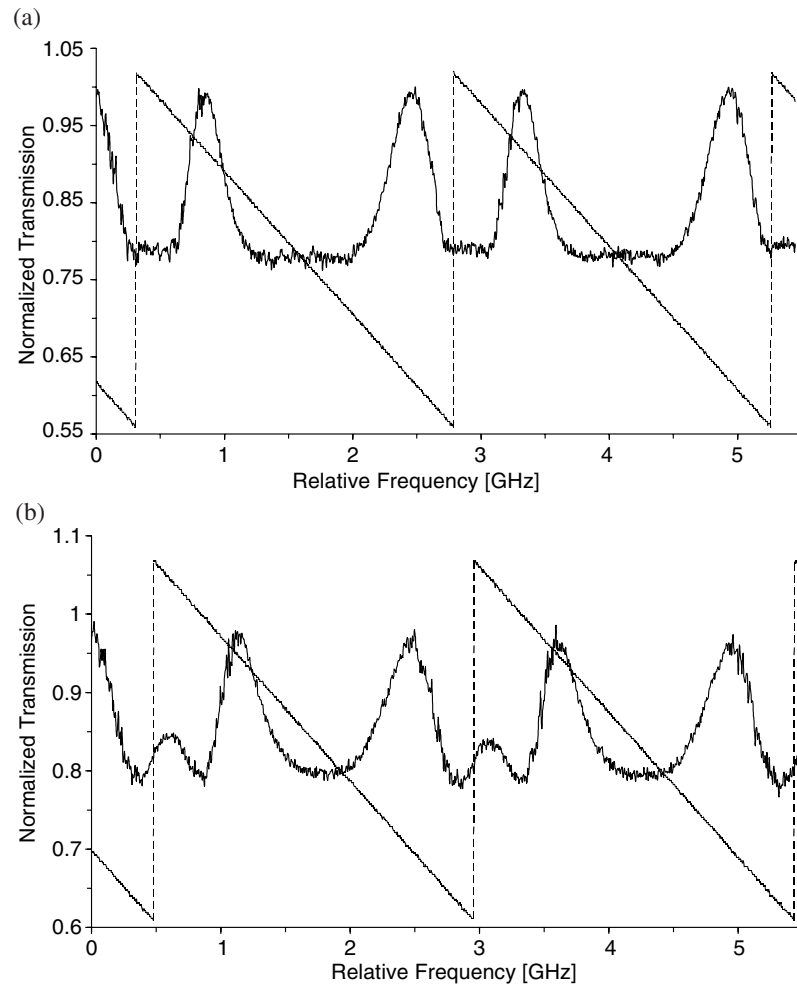
Figure 11. (a) The transfer function of a 63 mm cavity FP filter (——); sawtooth scan voltage applied to the filter (— — —). (b) The transfer function of figure 11(a) showing the effect of drift.
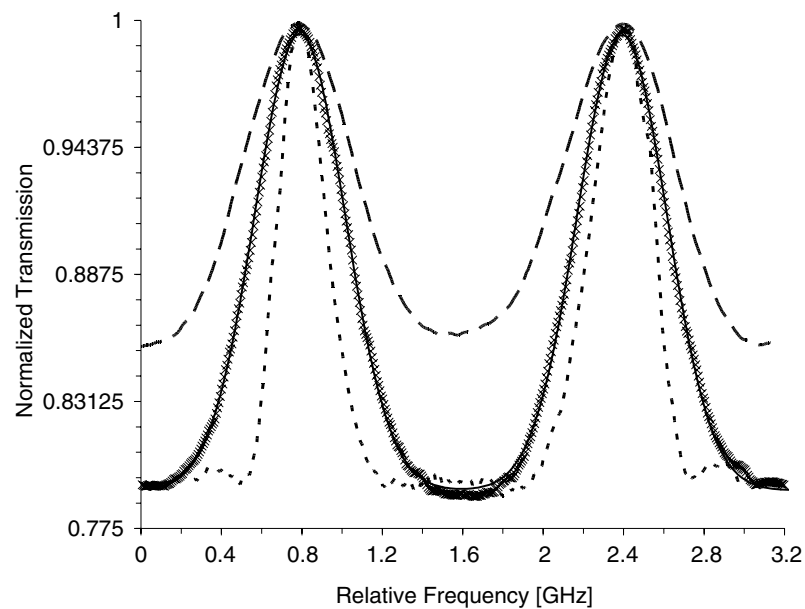
Figure 12. Experimental strain tuning of the FP transfer function that gives FWHM bandwidth and sensitivity respectively as: · · · · · ·, 0.27 GHz and 1.40 GHz^{-1}; ×, 0.51 GHz and 1.29 GHz^{-1} (with ——, Gaussian fit); — — —, 0.62 GHz and 0.5 GHz^{-1}. The visibility varies over a range of 15–22%.
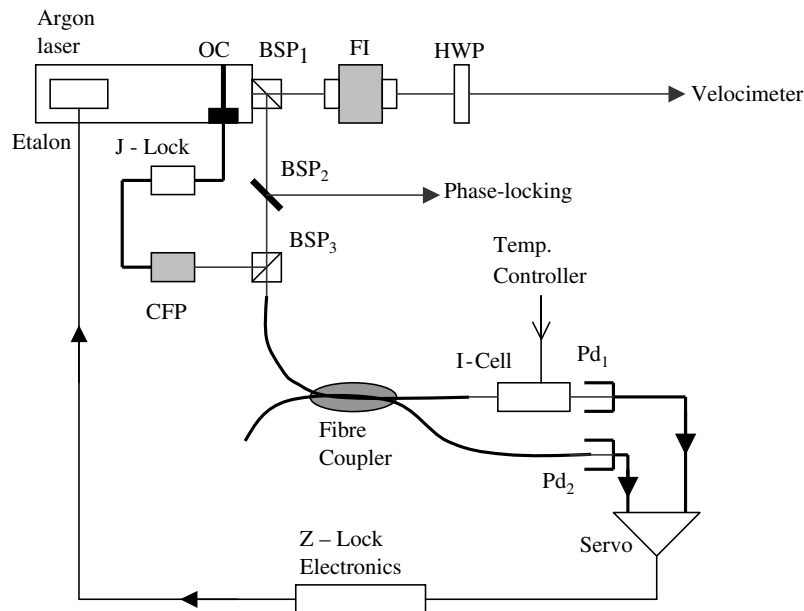
Figure 13. Schematic of an active wavelength stabilization system for the argon-ion laser: HWP, half-waveplate; BSP$_{1-3}$, beamsplitter cubes; Pd$_{1,2}$, photodiode detectors; I-cell, iodine cell; CFP, confocal FP interferometer; FI, Faraday isolator; OC, output coupler; J, feedback electronics that compensates for frequency jitter in the laser optical frequency.
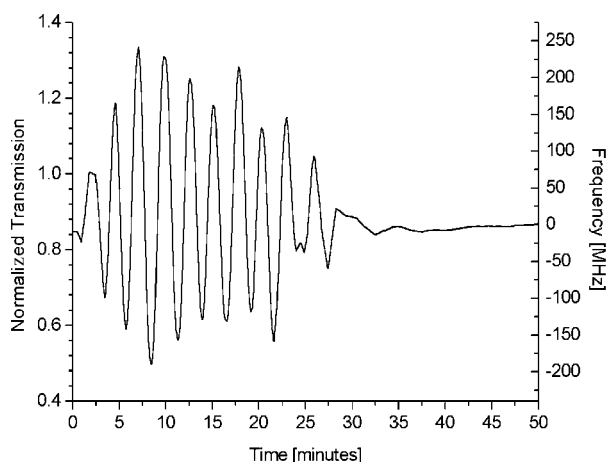
Figure 14. Response signal for the laser system under PID control in closed-loop feedback format.

stability. The integral time constant of the PID circuit was set at 1.12 and 0.2 s for the derivative action while the proportional factor gain of 25% was used for the proportional action. The laser could be brought into lock mode in about 10 min but higher stability was achieved by increasing this time, e.g. to 30 min as shown in figure 14. The laser could be locked to within ± 3 MHz (over a short timescale), which is equivalent to ± 0.6 m s^{-1} by using a full PID system.

3.3. Phase stabilization of the interferometer

The output of the fibre FP interferometer was found to drift with time, a consequence of thermally induced phase drift. The drift could be partly removed by using a thermal shield made out of polystyrene placed around the interferometer. The filter transfer function could be reset to its original form by applying a small offset strain to one grating using a function generator.

A simple feedback control system was therefore designed to lock the phase of the filter to the laser wavelength (figure 15). This scheme compensates for thermally induced phase changes and also relaxes the need to control the wavelength of the laser as the filter is automatically locked to track the laser wavelength. The scheme is based on phase detection with digital lock-in amplifiers (Stanford Research System SR850) and a custom-designed three-term electronic controller for adjusting the strain level applied to the filter gratings.

A small amount of light from the argon-ion laser ($< 1 \mu$W) was passed through an optical chopper at a frequency of 2 kHz (figure 15). The resulting pulse signal was coupled to one input arm of a single-mode fibre directional coupler at 514.5 nm wavelength having a split ratio of 50:50. The polarization state controller, PSC$_1$ enabled the linear polarization-state (vertical) of the input light to be matched to an eigenstate of the optical fibre by stress birefringence [32]. A polarization beamsplitter (PBS$_{1,2}$) placed at the output end of each arm of the coupler enabled the chopped signal to be detected by photomultiplier tubes PMT$_{sig}$ and PMT$_{ref}$ only. This automatically separated the chopped signal from the velocity signal that had been polarized orthogonally (horizontally) by use of PSC$_2$ in the second input arm of the coupler.

The signals, PMT$_{ref}$ and PMT$_{sig}$, were locked in phase by two digital lock-in amplifiers. The oscillator frequency that drives the chopper motor was connected to both lock-in amplifiers to provide a reference for locking purposes. The quality of phase detection was improved by using 24 dB/octave digital filters in the lock-in amplifiers and a time constant of either 100 or 300 ms. The voltage output of the lock-in amplifiers, proportional to phase, was divided using a software program written in LabView in a personal computer (PC).

A custom PID electronic circuit was set up to act upon the normalized lock-in amplifier signals that were output from the PC as an analogue signal. The circuit then generated an error
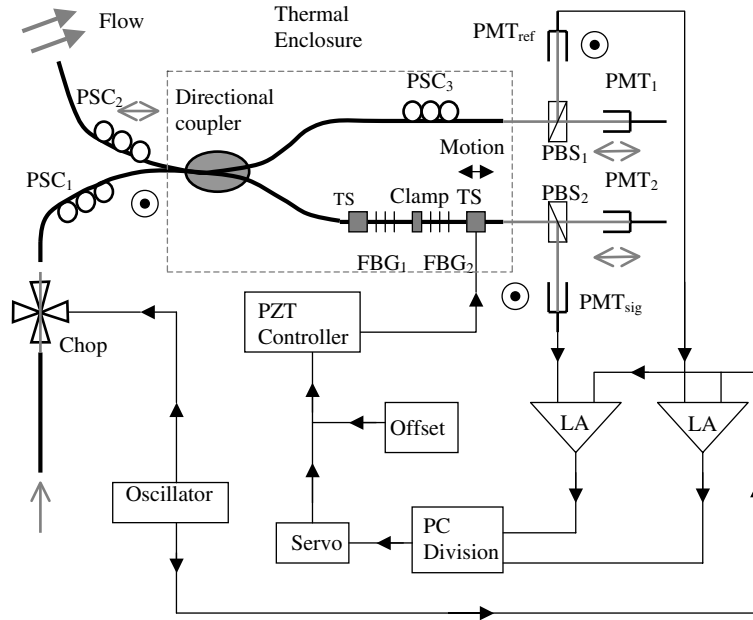
Figure 15. Schematic of an active phase stabilization system for a fibre FP filter: PSC_{1-3}, polarization state controllers; $PMT_{1,2}$, photomultiplier tubes; $PBS_{1,2}$, polarization beamsplitters; TS, translation stage; $FBG_{1,2}$, FBGs; LA, lock-in amplifier; PZT, piezoelectric transducer. $\odot$, vertically polarized light; $\leftrightarrow$ horizontally polarized light.
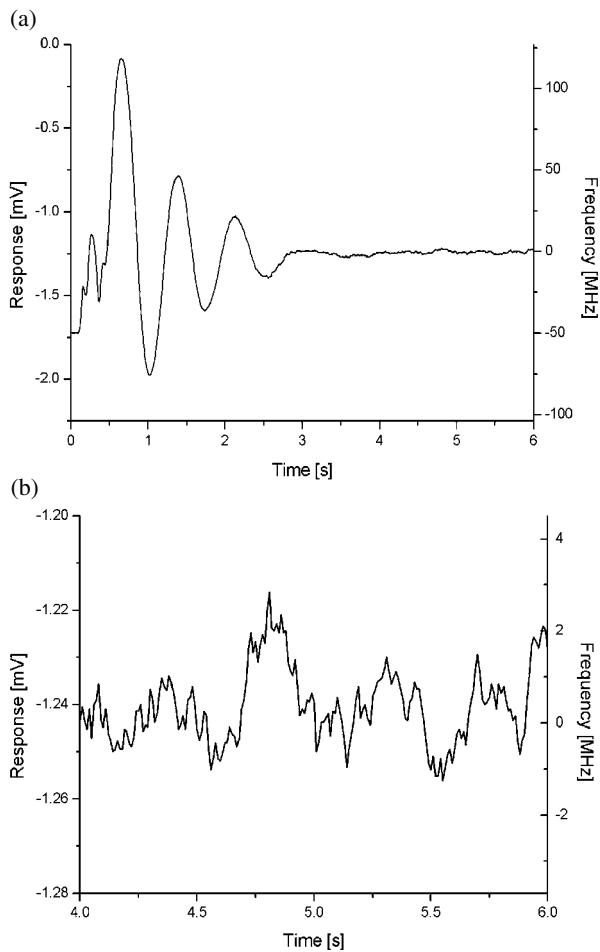

Figure 16. (a) Response signal for an FP filter under PID control in closed-loop feedback format. (b) Exploded frequency scale of figure 16(a) in the 4–6 s region (steady state of FP filter).

signal that was fed back to the piezoelectric-driven translation stage of the second FBG, FBG_2, via a piezoelectric transducer (PZT) controller. A feedback voltage of 17.3 mV moved the translation stage by 0.173 μm providing a π phase change in the FP interferometer. Mode hop free locking was ensured by limiting the frequency excursion to about 460 MHz, that is approximately a quarter of the FP FSR. This was achieved by limiting the feedback voltage modulation to 5 mV. A control voltage of ± 11 μV was required to achieve a ± 1 MHz frequency stability with a concomitant velocity resolution of about ± 0.2 m s^{-1}. An offset voltage on the PZT controller supplied by a function generator (Stanford Research Systems DS345) was used to tune the FP filter to a 50% transmission point of the transfer function, a requirement for directional discrimination in velocity.

The integral time constant of the circuit was 0.22 s, derivative time constant 0.04 s, and a proportional band of 77%. The performance of the control loop depends on how well tuned the individual P, I and D actions are, including their gain settings. Figure 16(a) is an example of the PID response when the system was in closed-loop feedback control mode while figure 16(b) is an insert of the exploded frequency scale of the same graph near the steady state. The system generally took about 0.5 s to stabilize to within 20 MHz and finally stabilized to within ± 3 MHz after 5 s. These times and stability margins, however, depended on the number of environmental perturbations and the controller settings. The required stability and resolution of ± 0.2 m s^{-1} was achieved by engaging both phase and laser wavelength stabilization.

3.4. Velocimeter configuration

Figure 17 is the velocimeter configuration incorporating drift compensation. About 1% of the laser output power was split off and a 10/90 beamsplitter cube further split this
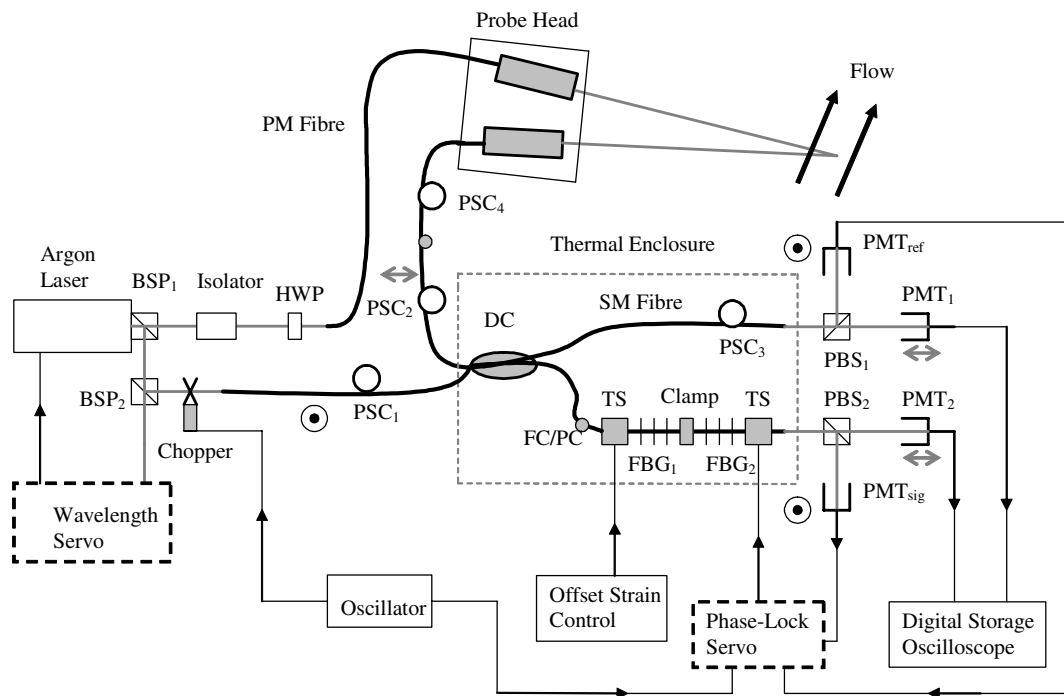
Figure 17. In-line fibre-optic LDV configuration: BSP_1, beam splitter cube (ratio 99/1); BSP_2, beamsplitter cube (90/10); HWP, half-waveplate; PM, polarization maintaining; PSC_{1-4}, polarization state controllers; DC, optical fibre directional coupler; SM, single mode; TS, translation stage; $FBG_{1,2}$, FBGs; $PBS_{1,2}$, polarization beamsplitter cubes; $PMT_{1,2}$, photomultiplier tubes for Doppler shift detection; $PMT_{ref,sig}$, photomultiplier tubes for phase locking of the interferometer. $\odot$, vertically polarized light; $\leftrightarrow$ horizontally polarized light.

beam to supply the optical signal for the phase-lock loop and wavelength servo.

The performance of the velocimeter was evaluated by measuring the velocity of a matt white painted rotating Perspex disc. Linearly polarized light from the laser was coupled into high-birefringence (Hi-Bi) optical fibre (Fibrecore HB450) aligned with the eigen-axis to preserve the state of polarization in the measurement volume. The ends of the optical fibres that connect to the probe head were angle polished at 8° and all other fibre ends in the system were flat-polished and connectorized by FC/PC connectors. Index-matching gel was also used where necessary. These precautions prevented the formation of any low-reflectivity optical cavities that could result in additional interferometers being set up in the system. The probe head (two-headed), designed and constructed in-house for turbomachinery applications [14], has a working distance of 400 mm and both heads operate at an f-number of 8. This produced a measurement volume of 70 μm width and 345 μm in length when the angle between the two heads was set at 20°.

The scattered light from the flow was coupled through the second input arm of the coupler. The polarization state, controlled by PSC_4, was set to be aligned orthogonal to the pulse signal and thus emerged horizontally polarized. This signal was detected by PMT_1 and PMT_2. PSC_2 is pre-aligned to give a horizontal polarization output to the detectors by coupling the laser light directly to this arm before the experiment. The separation of polarization in the output arms of the coupler decreases depending on the fibre deployment so PSC_3 was used to optimize the extinction ratio. The two signals were normalized and processed by a 300 MHz digital storage oscilloscope (Lecroy 9450A). The extinction ratio between the pulse signal and velocity signal was about 21 dB and this was

recorded with the disc stationary. The scattered light collected from the rotating disc was, however, completely depolarized regardless of the orientation of the incident linear polarization. Mie scattering theory from small particles predicts that the polarization of the scattered light is predominantly that of the incident beam. The depolarization was therefore considered to be a consequence of the nature of the paint used on the disc, particularly its particulate size.

A polarizer was placed in front of the receiver head and was rotated until the polarization of the signal was orthogonal to the pulse signal. Whilst producing the desired extinction ratio this resulted in the actual detected signal being attenuated thus reducing the signal to noise ratio. With the laser operating at 700 mW the collected signal from a stationary disc was about 100 nW and 30–50 nW for a rotating disc whose plane was set at an angle of about 36° to the central axis of the probe head. This provided sufficient signal for operating the velocimeter with the two-photomultiplier tube detectors set to medium gain values. A Mie scattering calculation shows that for a 0.5 μm diameter particle of refractive index 1.3 approximately 50 nW will be coupled into the receiving fibre indicating that the light levels used are commensurate with those from a single particle transit through the measurement volume. However, in contrast to LDV the method presented here can operate with higher densities of seeding particles which would produce larger scattered signals. The small residual cross-talk from the pulse channel on the velocity channels was minimized by lowering the intensity level of the pulse signal. Also, the gain on PMT_{sig} and PMT_{ref} was lowered so that they did not record the small cross-talk caused by the velocity signal onto the pulse channels. PMT_1 and PMT_2 had essentially identical responses and were therefore used for velocity measurements so that the
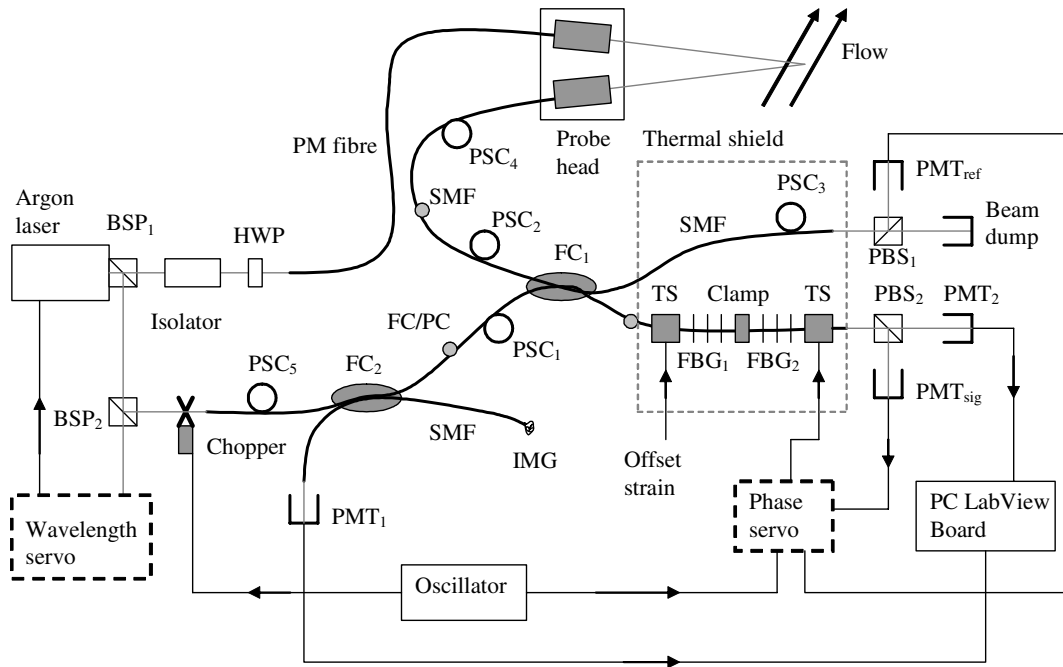
Figure 18. Fibre-optic laser Doppler velocimeter configuration for high sensitivity measurements: BSP_1, beamsplitter cube (ratio 99/1); BSP_2, beam splitter cube (90/10); HWP, half-waveplate; PM, polarization maintaining; PSC_{1-5}, polarization state controllers; $FC_{1,2}$, directional couplers; SMF, single-mode fibre; TS, translation stage; $FBG_{1,2}$, FBGs; $PBS_{1,2}$, polarization beamsplitter cubes; IMG, index-matching gel; $PMT_{1,2}$, photomultiplier tubes for Doppler shift detection; $PMT_{ref,sig}$, photomultiplier tubes for phase stabilization of the FP filter.

normalization remained accurate. PMT_{sig} and PMT_{ref} were matched to each other at a received power of 2 μW and were used for phase-locking purposes.

Independent velocity measurements of the rotating disc were made from measurements of the angular frequency. A stripe of a reflective tape was placed at the back of the disc and a laser beam from a miniature laser was directed onto the disc at the position of the tape with a photodetector positioned to receive the reflected light. The light reflected from the tape was modulated at the rotational frequency of the spinning disc and was measured on a dynamic signal analyser (Hewlett Packard 35660A). The recorded frequency was very stable, with the error in a single measurement being less than 0.25 Hz, which was improved to 0.02 Hz (equivalent to a velocity resolution of 0.008 m s^{-1}) by taking an average of 10 samples. The rotational frequency was recorded simultaneously with the disc velocity as measured by the velocimeter.

3.5. High-sensitivity velocimeter

The velocimeter configuration of section 3.4 was reconfigured to increase the instrument sensitivity, a unique attribute of the velocimeter presented in this work. Figure 18 shows the velocimeter reconfigured such that a reflected signal from the FP filter is detected by PMT_1 that was originally placed in transmission. All other components were left unchanged. The signal and locking signals were maintained orthogonal to each other using polarization state controllers, as in figure 15. The two fibre directional couplers were both of single-mode type at 514.5 nm wavelength and had a split ratio of 50:50. Losses through the system, e.g. the polarizer, second coupler and the connectors, resulted in a low signal that approached

the minimum detection sensitivity of the digital oscilloscope ($<$5 mV).

A simple configuration that did not incorporate the second coupler, phase stabilization mechanism and the polarizer sheet was adopted. The wheel geometry was also changed such that its plane made a large angle of 79° with the central axis of the probe head. These changes increased the strength of the signal that was collected from the measurement volume on the rotating disc. This increase in the included angle between the plane of the wheel and the optical axis also reduced the velocity measurement range. The gain of PMT_1 was increased for its signal to be comparable in magnitude to that of PMT_2. The digital storage oscilloscope was replaced by a PC installed with a LabView data acquisition board (PCI-MIO-16E-4) having a 12 bit resolution and a bandwidth of 600 kHz. The use of a PC enabled more information to be captured and analysed so that the true reflection and transmission signals were deduced from the known PMT gain. A thick polystyrene enclosure was used to shield the FP filter system from environmental perturbations particularly ambient temperature variations. The system was left to stabilize before taking measurements.

4. Results

### 4.1. Drift compensated velocimeter

The disc geometry gave a frequency to velocity coefficient of 2.73 MHz/m s^{-1}. The results were calculated by using both the gradient of the transfer function, which was 1.29 GHz^{-1}, as well as a polynomial curve-fit of degree 6 that was made to the transfer function. The velocity range measured by both methods, limited by the maximum rotation frequency of the
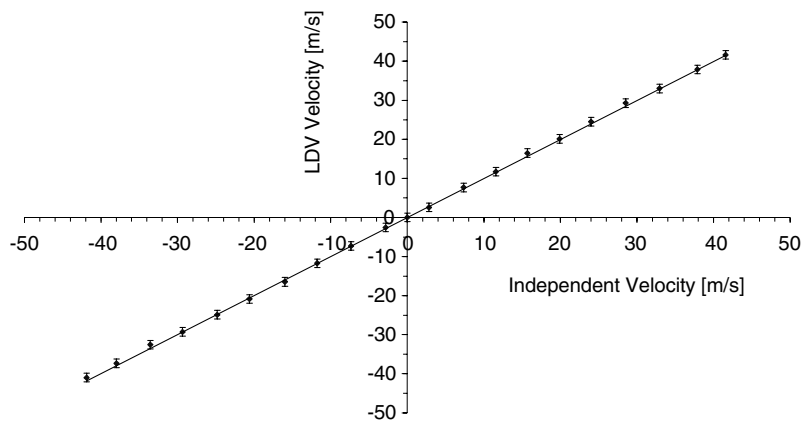
Figure 19. Disc velocity measured by the velocimeter configuration of figure 17 plotted against the disc velocity measured using its angular frequency. The gradient of the line is 1.005 ± 0.002.
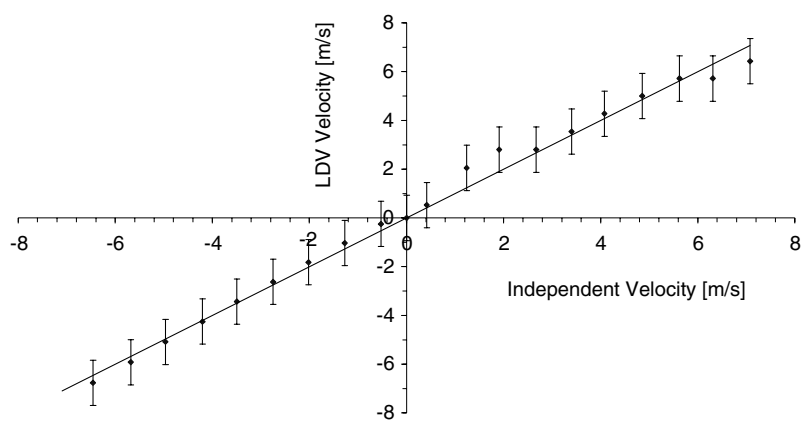
Figure 20. Disc velocity measured by the velocimeter configuration of figure 18 plotted against the disc velocity measured using its angular frequency. The gradient of the line is 1.00 ± 0.02.

disc, was ± 42 m s^{-1} with a resolution of 0.2 m s^{-1}. Figure 19 shows the results obtained by using the gradient of the transfer function. The gradient, m, of the transfer function is used to obtain the Doppler frequency shift, $\Delta \nu$, by

$$\Delta \nu = \frac{\Delta T}{m} \qquad (3)$$

where ΔT is the change in transmission intensity. This Doppler shift is used in equation (2) to obtain the required velocity. The gradient of figure 19 is 1.005 ± 0.002 while that of the velocity obtained from a polynomial fit is 0.998 ± 0.004 which are respectively 0.5 and 0.2% deviation from the expected line.

4.2. High-sensitivity velocimeter

The Doppler frequency to intensity conversion factor for the disc geometry was 1.35 GHz^{-1}, given by the gradient of the filter transfer function. The velocity measurement range was ± 7 m s^{-1} with a resolution of 0.2 m s^{-1} (figure 20) and the Doppler frequency shift to velocity coefficient for the velocimeter configuration was 0.73 MHz/m s^{-1}. There is a noticeable drift in the graph, particularly in the positive velocity quadrant, which is a consequence of the signal drift of the velocimeter since the phase-locking system was suspended

for the reasons discussed in section 3.5. However, a plot of the negative quadrant velocities alone gave a linear graph of gradient 1.104 ± 0.006, which is consistent with the phase drift of the filter since measurements were started from the negative end before this drift had taken effect.

5. Discussion

The results demonstrate that this velocimeter is versatile and has several benefits that are derivable from it. Varying instrument sensitivities were obtained by strain-tuning the fibre FP filter but the results presented had the gradient of the transfer function tuned to 1.29 and 1.35 GHz^{-1}. The back reflection configuration presented a unique attribute of the velocimeter that doubled the instrument's sensitivity enabling lower velocity measurement using the same filter. A low velocity range of ± 7 m s^{-1} was therefore measurable from a previous measurement of ± 42 m s^{-1} and the resolution was 0.2 m s^{-1}. The velocity range for the velocimeter can be significantly increased by increasing the FSR of the filter, e.g. a 3 GHz FSR for a filter fabricated with a finesse of 3.3 (40% Bragg grating reflectivity) would give a velocity range of more than 350 m s^{-1}. Similarly a combination of small FSR and high finesse enable smaller velocity ranges to be measured limited only by the optical frequency stability of the filter response and laser output.

In all the measurements it was the filter that was tuned to the laser wavelength such that automatic directional velocity discrimination was achieved. This is a significant advantage when compared with the use of an iodine cell, which requires a tuneable laser source since the filter itself cannot be tuned. The velocimeter was designed around the use of an argon-ion laser but in principle any laser wavelength source can be used provided the filter, e.g. the Bragg grating FP interferometer, DFG or moiré grating, is fabricated at the preferred wavelength of the source. Such versatility would be important, particularly where miniaturization of instrument components may be paramount as miniature high-power laser diode sources and solid state lasers are now available.

6. Conclusion

A non-intrusive fibre-optic in-line laser Doppler velocimeter based on a Bragg grating FP interferometer as a frequency to intensity transducer has been presented. Two independent feed back control loops were designed to actively compensate for the phase variations in the FP interferometer and laser wavelength fluctuations. The velocimeter successfully made measurements over the full range that was available in the laboratory (85 m s^{-1}) with a resolution of 0.2 m s^{-1}.

Acknowledgment

References

[1] Yeh Y and Cummins H Z 1964 Localised fluid flow measurements with a He–Ne laser spectrometer *Appl. Phys. Lett.* **4** 176–8

[2] Goldstein R J and Kreid D K 1967 Measurement of laminar flow developed in a square duct using a laser Doppler flowmeter *J. Appl. Mech.* **34** 813–18

[3] Vom Stein H D and Pfeifer H J 1969 A Doppler difference method for velocity measurements *Metrologia* **5** 59–61

[4] James S W, Tatam R P and Elder R L 1997 Design considerations for three dimensional fibre-optic laser Doppler velocimeter for turbomachinery applications *Rev. Sci. Instrum.* **68** 3241–6

[5] Schodl R and Forster W 1988 A multi colour fibre optic laser two focus velocimeter for 3-dimensional flow analysis *AIAA paper*-88-3034 *(July 1988)*

[6] Ahmed N A, Hamid S, Elder R L, Forster C, Tatam R P and Jones J D C 1992 Fibre optic laser anemometry for turbomachinery applications *Opt. Lasers Eng.* **16** 193–205

[7] Dancey L 1987 A review of three-component laser Doppler anemometry *J. Opt. Sensors* **2** 437–69

[8] Snyder P K, Orloff K L and Reinath M S 1984 Reduction of flow-measurement uncertainties in laser velocimeters with nonorthogonal channels *AIAA J.* **22** 1115–23

[9] Ross M M 1997 Combined differential and reference beam LDV for 3D velocity measurement *Opt. Lasers Eng.* **27** 587–619

[10] Chan V S S, Heyes A L, Robinson D I and Turner J T 1995 Iodine absorption filters for Doppler global velocimetry *Meas. Sci. Technol.* **6** 784–94

[11] Komine H, Brosnan S J, Litton A B and Stappaerts E A 1991 Real-time Doppler global velocimetry *29th Aerospace Sciences Mtg (Reno, 1991) AIAA Paper*-91-0337

[12] Meyers J F 1992 Doppler global velocimetry. The next generation *17th Aerospace Ground Testing Conf., (Nashville, TN, 1992) AIAA Paper* 92-3897

[13] Roehle I, Karpinski G and Schodl R 1999 3-component-Doppler laser-two-focus: a new kind of three component velocimeter *18th Int. Conf. on Instrumentation in Aerospace Simulation Facilities ICIASF 99 (Toulouse Cedex)* pp 13.1–13.9

[14] Egan D A, James S W and Tatam R P 1997 On-axis laser Doppler velocimetry for turbomachinery applications using optical fibre techniques *Proc. SPIE: Optical Technology in Fluid, Thermal, and Combustion Flow 111* vol 3172 pp 17–26

[15] Hoffenberg R and Sullivan J P 1993 Filtered particle scattering: laser velocimetry using an iodine filter *ASME-FED Fluid Meas. Instrum.* **161** 135–8

[16] Kuhlman J M, Naylor S, James K and Ramanath S 1997 Accuracy study of a 2-component point Doppler velocimeter *28th Fluid Dynamics Conf. (Snowmass Village, CO, 1997) AIAA Paper* 97-1916

[17] James S W, Lockey R A, Egan D and Tatam R P 1995 Fibre optic based reference beam laser Doppler velocimetry *Opt. Commun.* **119** 460–4

[18] Byrne G D, James S W and Tatam R P 2001 A Bragg grating based fibre optic reference beam laser Doppler anemometer *Meas. Sci. Technol.* **12** 909–13

[19] Kashyap R 1999 *Fibre Bragg Gratings* (London: Academic)

[20] Othonos A 1997 Fiber Bragg gratings *Rev. Sci. Instrum.* **68** 4309–41

[21] Yamada M and Sakuda K 1987 Analysis of almost-periodic distributed feedback slab waveguides via a fundamental matrix approach *Appl. Opt.* **26** 3474–8

[22] Erdogan T 1997 Fibre grating spectra *J. Lightwave Technol.* **15** 1277–94

[23] Legoubin S, Douay M, Bernage P, Niay P, Boj S and Delevaque E 1995 Free spectral range variations of the grating-based Fabry–Perot filters photowritten in opticalfibres *J. Opt. Soc. Am.* A **12** 1687–94

[24] Kashyap R, Mckee P F and Armes D 1994 UV written reflection grating structures in photosensitive optical fibres using phase-shifted phase masks *Electron. Lett.* **30** 1977–8

[25] Zhang L, Sugden K, Bennion I and Molony A 1995 Wide-stopband chirped fibre moiré grating transmission filters *Electron. Lett.* **31** 477–9

[26] Canning J and Sceats M G 1994 π-phase-shifted periodic distributed structures in optical fibres by UV post-processing *Electron. Lett.* **30** 1344–5

[27] Dockney M L, James S W and Tatam R P 1996 Fibre Bragg gratings fabricated using a wavelength tuneable laser source and a phase mask based interferometer *Meas. Sci. Technol.* **7** 445–8

[28] Armstrong B H 1967 Spectrum line profiles: the Voigt function *J. Quant. Spectrosc. Radiat. Transfer* **7** 61–88

[29] Vaughan J M 1989 *The Fabry–Perot Interferometer* (Bristol: Hilger)

[30] Heilmann R and Kuschel J 1993 Absolute frequency locking of diode-pumped Nd: YAG laser for application in free-space optical communication *Electron. Lett.* **29** 810–11

[31] Nobes D S, Ford H D and Tatam R P 2002 Three component planar Doppler velocimetry measurement using imaging fibre bundles *11th Int. Symp. on Applications of Laser Techniques to Fluid Mechanics (Lisbon, Portugal, July 2002)*

[32] Lefevre H C 1980 Single-mode fibre fractional wave devices and polarisation controllers *Electron. Lett.* **16** 778–80